CYCLIC SHEAR BUCKLING OF THIN-WALLED ALUMINIUM PANELS

P.Horst and H.Kossira

Institut für Flugzeugbau und Leichtbau (IFL)
(Institute for Aircraft Design and Structural Mechanics)
Technical University Braunschweig, FR Germany

Abstract

A theoretical and experimental study, which represents the first phase of a more comprehensive program on the postbuckling behaviour of clamped aluminium-plates subjected to cyclic shear-load, is presented. The applied load exceeds the theoretical buckling load by a factor of 20 to 40; moderate plastic deformations occur. The aim of the study is a better understanding of the occuring phenomena and a verification of the theoretical model. This model is based on the finite element method, it is capable of calculating the nonlinear postbuckling behaviour, taking into account material nonlinearities. Emphasis is layed on a good approximation of the cyclic elasto-plastic stress-strain-relation of 2024 T3 (resp. T351). A multisurface-model and a *Mróz*-type translation-rule yields good results. Apart from the theoretical model, the main objectives of this paper are: imperfection sensitivity, plastic zones, load reversal behaviour, load-deflection-curves, highly stressed regions and results of low-cycle-fatigue-tests.

Nomenclature

a Plate-dimension

a_i Anisotropy parameter

$\mathbf{C}$ Matrix of the in-plane, coupling and bending stiffnesses

E Material stiffness

F Area of the plate midsurface

$m^{\alpha\beta}$ Bending moment

$n^{\alpha\beta}$ Membran force

n_{ij} Outward normal of the yield or bounding surface

N Number of loading cycles

P Tensile force of the hydraulic cylinder

$\bar{p}$ Discrete force vector

$\mathbf{Q}$ Inverse matrix of $\mathbf{C}$

t Plate-thickness

u_3^c Central displacement of the buckled plate

$\mathbf{v}$ Vektor of the displacements u_i

α^{ij} Back-stress tensor of the yield-surface

$\bar{\gamma}$ Angle of shear

δ First variation

ε_{ij} Strain-tensor (Green-Lagrange)

κ Yield-stress

σ^{ij} Stress-tensor (2. Piola-Kirchhoff)

ϕ yield function

Indices

$^{\Delta}( )$ Finite step

$^{o}( )$ Initial state

$^{t}( )$ State "t"

$( )^{L}$ Linear part

$( )^{N}$ Nonlinear part

$( )_{,\alpha}$ Derivation with respect to α

$( )^{(l)}$ Variable of the l^{th}-surface

$( )^{(el)}$ Elastic part

$( )^{(max)}$ Maximum of ( )

$( )^{(min)}$ Minimum of ( )

$( )^{(pl)}$ Plastic part

1. Introduction

Plates and curved panels subjected to shear are widely used in aircraft and spacecraft structures. They exhibit a stable postbuckling behaviour and are able to sustain loads far in excess of their initial buckling limits, i.e. critical load and by using this higher postbuckling range, essential weight savings are possible. This statement is also valid, if moderate plastic deformations occur. Although the plastic limit may not be reached in aircraft structures under normal conditions, it may be exceeded to some extent in emergency cases. For instance in fail-save cases, since moderate plastic deformations are allowed, low-cycle-fatigue has to be expected.

Moreover it is of interest to validate the used numerical model by comparison with experimental results. For this reason the case of the shear-loaded plate has been investigated by some authors. E.g. SINGER ET AL. [1+2] used a Wagner-beam-like test set-up for the experimental investigation of crack initiation, propagation and failure. In

this case some problems arise with regard to theoretical assumptions since boundary conditions can not be determined exactly. A test set-up with clamped edges producing *pure* shear circumvents this problem and the boundary conditions can be realized experimentally and theoretically in a finite element model. It is possible to show that the difference between clamped and simply supported boundary conditions nearly vanishes in the higher postbuckling range [3]. A reasonable comparison of both experimental and theoretical results can be achieved and conclusions on the suitability of the mechanical model can be made. The special, clamped problem has been examined for the monotonic loading case by TUNKER [4] for GFRP plates and by WOLF and KOSSIRA [5] for CFRP shells, both also taking into account material nonlinearities.

Simple, isotropical material laws (including pure isotropic hardening) yield poor theoretical results if unloading and reloading of the plates are concerned. Better results are found by applying more sophisticated multi-surface models, which also include the pretreatment of the sheets. The problem of cyclically shear-loaded aluminium plates has been treated in [6] by the authors employing a modified Dafalias-Popov-model [7]. Other, more sophisticated models have been used, but did not lead to better results [3]. In this paper a *Mróz*-type model [8] has been employed. As shown in [3] this model yields better results, due to the fact that high non-proportional stress-paths are found in case of cyclic shear buckling. The computational effort and in particular the storage capacity needed by this model are relativly small. This model yields a good approximation of measured uniaxial stress-strain characteristics and is also able to take into account initial plastic orthotropy due to the prestraining treatment of the material.

Theoretical investigations have been carried out by the finite element code FIPPS of the Institut für Flugzeugbau und Leichtbau [9]. It uses a mixed formulation of the elements. This kind of formulation produces displacements and stresses with the same degree of approximation as primary unknowns. This procedure also has some advantages concerning mostly the numerical effort for the computation of the geometrical nonlinearity.

2. The Theoretical Model

In this part some basic proposals, concerning the FE-formulation and the material model, are made. The following theory is valid for quasi-static, isothermal problems.

2.1 The Finite Element Formulation

Finite deformations and moderate rotations, but only small strains are admissible and a *Total Lagranien* formulation has been adopted. The aspect ratio of the plates in this study is high enough to use a *Kirchhoff-Love*-type theory. A *Mindlin*-theory is not attractive here, since there are certain inconsistencies in case of elasto-plastic deformations [3] and the computational effort would be about 50 % higher. Fig.1 shows the definition of the mechanical vector quantities. Latin letters run from 1 to 3 and greek letters from 1 to 2, indicating quantities of the midsurface of the plate. For a certain state "l" the incremental mixed workprinciple reads ([3,5])

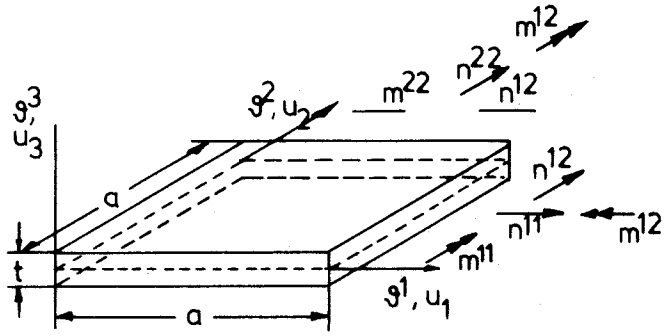

FIG. 1: Definition of mechanical properties

$$\delta^{\Delta}A = 0$$

$$= -\int_F [\delta^{\Delta}n^{\alpha\beta}\,{}^{\Delta}\alpha^{L}_{\alpha\beta} + \delta^{\Delta}m^{\alpha\beta}{}_{,\beta}\,{}^{\Delta}u_{3,\alpha} +$$

$$ {}^{\Delta}n^{\alpha\beta}\delta^{\Delta}\alpha^{L}_{\alpha\beta} + {}^{\Delta}m^{\alpha\beta}{}_{,\beta}\delta^{\Delta}u_{3,\alpha} -$$

$$\{\delta^{\Delta}n^{\alpha\beta}(Q^{M}_{\alpha\beta\gamma\delta}\,{}^{\Delta}n^{\gamma\delta} + Q^{C}_{\alpha\beta\gamma\delta}\,{}^{\Delta}m^{\gamma\delta}) +$$

$$\delta^{\Delta}m^{\alpha\beta}(Q^{C}_{\alpha\beta\gamma\delta}\,{}^{\Delta}n^{\gamma\delta} + Q^{B}_{\alpha\beta\gamma\delta}\,{}^{\Delta}m^{\gamma\delta})\}]\,dF \quad (1)$$

$$-\int_F [\delta^{\Delta}n^{\alpha\beta}\,{}^{l}\alpha^{Ng}_{\alpha\beta} + {}^{\Delta}n^{\alpha\beta}\delta^{l}\alpha^{Ng}_{\alpha\beta} + {}^{l}n^{\alpha\beta}\delta^{\Delta}\alpha^{Ni}_{\alpha\beta}]dF$$

$$-\int_F [\delta^{\Delta}n^{\alpha\beta}\,{}^{\Delta}\alpha^{Ni}_{\alpha\beta} + {}^{\Delta}n^{\alpha\beta}\delta^{\Delta}\alpha^{Ni}_{\alpha\beta}]dF$$

$$+\int_F {}^{\Delta}\bar{p}^{i}\,{}^{\Delta}u_i dF$$

where

$${}^{\Delta}\alpha^{L}_{\alpha\beta} = \frac{1}{2}({}^{\Delta}u_{\alpha,\beta} + {}^{\Delta}u_{\beta,\alpha}) \quad (2a)$$

$${}^{\Delta}\alpha^{Ni}_{\alpha\beta} = \frac{1}{2}({}^{\Delta}u^{\rho}{}_{,\alpha}\,{}^{\Delta}u_{\rho,\beta} + {}^{\Delta}u^{3}{}_{,\alpha}\,{}^{\Delta}u_{3,\beta}) \quad (2b)$$

$${}^{l}\alpha^{Ng}_{\alpha\beta} = ({}^{\Delta}u^{\rho}{}_{,\alpha}\,{}^{l}u_{\rho,\beta} + {}^{\Delta}u^{3}{}_{,\alpha}\,{}^{l}u_{3,\beta}) \quad (2c)$$

denote the three parts of the membrane-strain. As the terms of the first integral of eqn 1 only contain linear expressions, this is equivalent to the parts of the linear stiffness-matrix. The second integral includes the terms of the tangent-matrix and the third integral represents the secant-matrix. The last matrix is used to determine the *out-of-balance-force* due to the geometric nonlinearity for a certain step "Δ". The effect of material nonlinearities is included in the tangent matrix (as $\mathbf{Q}$ depends on the state "t") and can also be detected as an *out-of-balance-force* for a finite step "Δ". As usual in this context, the nonlinear parts of the bending-strains have been neglected. ${}^{t}\mathbf{Q}$ denotes the inverse of the material stiffness ${}^{t}\mathbf{C}$. The inplane, coupling and bending stiffnesses of the plate material are determined by integration of the actual elasto-plastic tangent-moduli over the plate thickness. In this study the panel has been approximated by 10 discrete layers in the ϑ^3-direction. This approach is superior to integral models, if at least cyclic loading is concerned. By this method the effort of the description of the material behaviour is reduced to the case of the plain-stress constitutive

relation in each layer (see 2.2).

Since the numerical problem represented in eqn. 1 is nonlinear, a solution is only possible by incremental procedures. For further details see [3,5].

2.2 The Constitutive Relation

For a good approximation of the yield behaviour of a typical aluminium alloy, a *Mróz*-type model has been adopted. This model is based on classical rate-independent plasticity, so it only includes isothermal, room-temperature problems and small strains (effective strain $\leq 2\%$). For the definition of the set-on of plastic deformations and their direction and magnitude, the modified *v.Mises* yield-surface

$$\phi = \frac{1}{2}\Big(\frac{2}{3}a_1(\sigma^{11})^2 + \frac{2}{3}a_2(\sigma^{22})^2 - \frac{2}{3}a_{12}\sigma^{11}\sigma^{22} + \frac{6}{3}a_3(\sigma^{12})^2\Big) - \frac{1}{3}\kappa^2 \qquad (3)$$

is used. a_i are the anisotropy-parameters denoting the relation of the square of the yield-surface in one direction to the square of κ. (In the isotropic case $a_1 = a_2 = a_{12} = 1$ and $a_3 = 3$..) The yield surface moves in the stress-space by means of a *back-stress*-tensor α^{ij} directing from the origin of the stress space to the center of the yield surface. This process is called kinematic hardening. A second effect, called *isotropic hardening*, is included by means of a variable generalized yield stress κ, depending on *plastic internal variables*, e.g. the accumulated plastic strain. By using ϕ from eqn 3 as a plastic potential, the plastic strain increment is defined as

$$d\varepsilon_{ij}^{(pl)} = d\lambda\frac{\partial\phi}{\partial\sigma^{ij}}. \qquad (4)$$

According to this rule, the direction of the plastic strain increment is given by the gradient of the plastic potential; this is called the *normality rule*. λ is a *Lagrangien multiplier*, its size is ruled by the fact that the elasto-plastic stress-strain-relation always must be compatible. Since only small strains are allowed, an additive decomposition of the increment of the strain-tensor (Prandtl-Reuss)

$$d\varepsilon_{ij} = d\varepsilon_{ij}^{(pl)} + d\varepsilon_{ij}^{(el)} \qquad (5)$$

is used.

2.2.1 The Multisurface model. The Mróz model includes two main ideas. Firstly, the results of onedimensional tension-compression-tests are approximated by n linear parts. Within each part (index "l") a constant plastic tangentmodulus ${}^{(pl)}E^{(l)}$ is given. In case of multiaxial loading the domains of a constant elasto-plastic tangentmodulus are given by n different surfaces $\phi^{(l)}$ of different size $\kappa^{(l)}$. If for all surfaces $(\alpha^{ij})^{(l)} = 0$ in the virgin state of the material and no isotropic hardening is taken into account, a real *Masing*-effect is given by this model. This means that the onedimensional $\sigma - \varepsilon$-curve of the first loading is stretched by a factor 2 after load reversal.

During loading a surface does not move, until it is reached by the stress state. Since a surface can not be penetrated, it either has to move (kinematic hardening) or to grow (isotropic hardening) if there is plastic loading. An intersection of surfaces may not occur, as no appropriate plastic tangentmodulus could be found in this case. Thus Mróz second idea was a translation-law that fits this requirement. For a given stress state $(\sigma^{ij})^{(l)}$ on the surface (l), this is achieved by enforcing that the surface will move into a direction of a virtual stress state, where the virtual stress has the same outward normal on $\phi^{(l+1)}$ as $(\sigma^{ij})^{(l)}$ has on $\phi^{(l)}$.

All surfaces are of affine geometry, since all are ruled by eqn 3, so $(\sigma^{ij})^{(l+1)}$ may be computed by

$$(\sigma^{ij})^{(l+1)} = \frac{\kappa^{(l+1)}}{\kappa^{(l)}}\Big((\sigma^{ij})^{(l)} - (\alpha^{ij})^{(l)}\Big) + (\alpha^{ij})^{(l+1)}. \qquad (6)$$

After $(\sigma^{ij})^{(l)}$ is known, it is possible to determine the increment of the back-stress-tensor by

$$d(\alpha^{ij})^{(l)} = \frac{<n_{kl}\,d(\sigma^{kl})^{(l)}> - <d\kappa^{(l)}>}{n_{kl}\left((\sigma^{kl})^{(l+1)} - (\sigma^{kl})^{(l)}\right)}\Big((\sigma^{ij})^{(l+1)} - (\sigma^{ij})^{(l)}\Big) \qquad (7)$$

The brackets $< >$ indicate that these terms are nonzero only in case of plastic loading, n_{kl} is the unit-outward-normal on the surface. This translation-rule makes sure that both surfaces lay tangential to each other when they get into contact. As the inner surface is smaller than the outer, an intersection of both is avoided.

2.2.2 The applied material model. Specimens were made of the aluminium alloy 2024 with the pretreatment T3 or T351. In both cases the plates are solution heat treated, *cold worked* and naturally aged. The difference between T3 and T351 is the given limit of straining. The cold working treatment consists in rolling and prestraining of the sheet material. Caused by the pretreatment, the mechanical properties are orthotropic. While this orthotropy is neglectable in the elastic range, it is not at all in the plastic range. The variation of mechanical properties in the through-thickness-direction, due to the rolling treatment, has been neglected. Essential for good theoretical results of the cyclic shear-buckling problem is a good approximation of the yield behaviour for small plastic strains. Other, even more sophisticated models, have been tested in [3] but they did not yield essentially better results.

The model introduced in 2.2.1, is capable to approximate the uniaxial stress-strain curves of 2024 T351 for the case of small plastic strains. The major aim of this process is to fit well the material behaviour with special regard to the load direction. This aim is reached as follows: for a virtual virgin state, all surfaces are thought to lay concentric around the origine of the stress space. Due to the pretreatment isotropic and kinematic hardening occurs and the inner surfaces are moved (see fig 2). By this method a sharp kink of the stress-strain-curve is achieved in the vicinity of the yield-stress, if a tension is applicated in the L-direction of the plate-material. The stress-strain-curves of all other directions show a much more moderate relation. This approximates the real stress-strain-behaviour of 2024 T3 (resp. T351) very well. For simplicities sake and computational effort, only four surfaces have been used in this study. Characteristic points of the surface have been taken from tension- and compression-tests. The surfaces have been designed by accepting that all are modified v.Mises surfaces (see eqn 3). Tab 1 shows the parameters of the 4 surfaces used.

- yield-surface 1 : $\kappa^{(1)} = 265$ MPa , ${}^{t}E^{(1)}_{(pl)} = 84\,816$ MPa
- yield-surface 2 : $\kappa^{(2)} = 310$ MPa , ${}^{t}E^{(2)}_{(pl)} = 15\,185$ MPa
- yield-surface 3 : $\kappa^{(3)} = 375$ MPa , ${}^{t}E^{(3)}_{(pl)} = 1\,000$ MPa
- yield-surface 4 : $\kappa^{(4)} = 400$ MPa , ${}^{t}E^{(4)}_{(pl)} = 1\,000$ MPa

TAB. 1: Parameter of surfaces 1 to 4

Due to the prestress, surfaces (1) and (2) are moved in the stress space ($\alpha^{11(1)} = 100\,MPa$, $\alpha^{11(2)} = 45\,MPa$). Since measurements in the $\sigma^{11} - \sigma^{12}$-plane show a significant decrease of the yield-stress in σ^{12}-direction compared to the one predicted by the v.Mises surface, the anisotropy-coefficient a_3 has been increased from 3.0 to 3.3. The Youngs modulus amounts ${}^{(el)}E = 73000\,MPa$ with a Poisson ratio of $\nu = 0.31$.

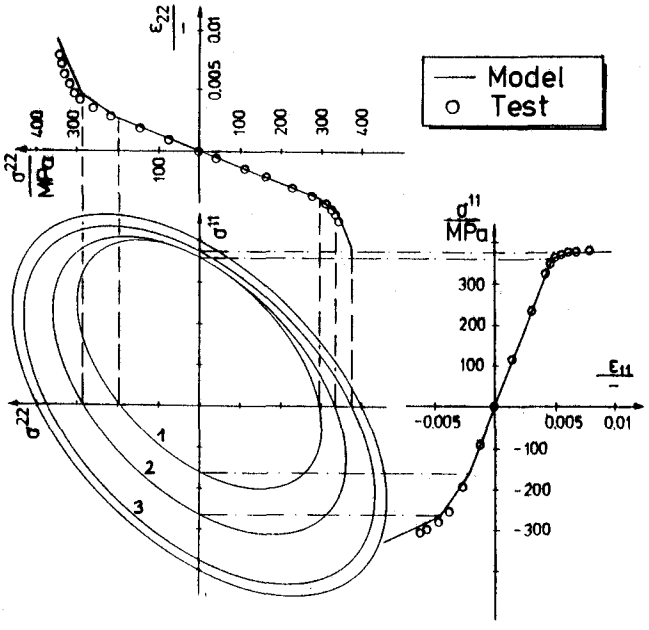

FIG. 2: Stress-strain relations of the Mróz-model (material 2024 T3).

3. Test set-up, tests and results

3.1 The test set-up

The test set-up is shown in Fig. 3. The force is applied by a hydraulic cylinder (250 kN) and is transformed into shear-load on the test panel by means of a shear-frame. The edges of the frame are pin-jointed, whereby the pins are located exactly in the corners of the square plate. The test-panel is not penetrated since the pin-joints are parted in the middle. This kind of arrangement differs from that used by others (e.g. in Ref. [10]). The test-frame has been chosen to be very stiff with the intention of minimizing deformations of the frame and gaining nearly *pure* shear.

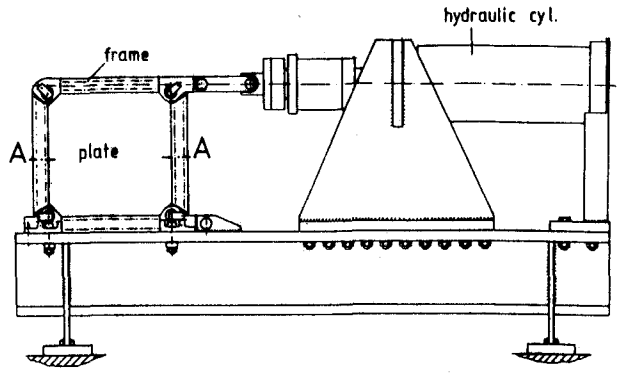

FIG. 3: Test set-up

There are three possible parameters suitable for the description of the global behaviour of buckling shear-panels: the force P of the hydraulic-cylinder, the angle of shear $\bar{\gamma}$ and the central deflection u^{ξ}_{3}. The central deflection u^{ξ}_{3} must always be linked to the corresponding buckling mode. The value of the force P of the hydraulic cylinder is partly absorbed by friction in the pin-joints of the test-frame, for this reason P is not a well suited parameter. Since the comparison of experimental and theoretical results needs at least one global load-parameter, the angle of shear $\bar{\gamma}$ is used as the appropriate parameter.

The angle of shear has been determined by means of inductive displacement transducers or a mechanical measuring set between the legs of the frame. Initial geometric imperfections and the buckling mode in the line A - A (Fig. 3) were determined by a deflection transducer which was attached to a carriage running on a slideway and connected to a x-y-recorder. In some cases the entire displacement field has been measured by means of engineering photogrammetry. Strain gauge rosettes positioned on both sides of the specimen opposite to each other were used to measure strains as local parameters, in order to enable a good comparison of experimental and theoretical results.

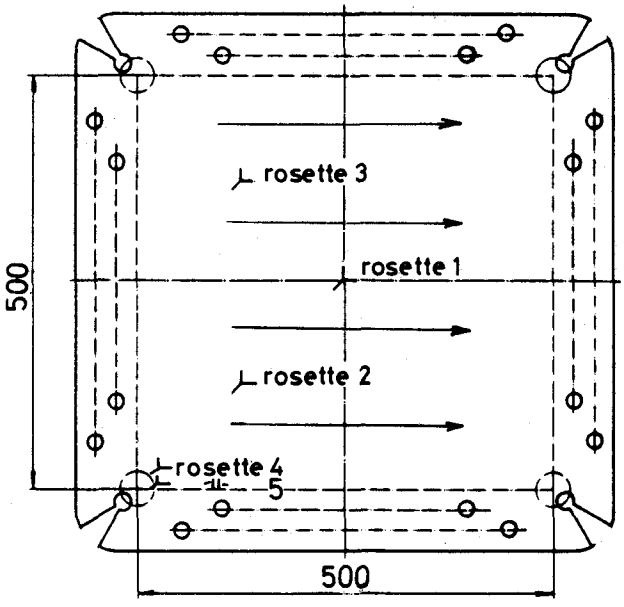

FIG. 4: The test panel and the contour of the "picture frame" test set-up

In this investigation thin-walled plates of 2024 T3, resp. T351 with the dimensions of 500 x 500 mm^2 were used. The shape of the entire test-panel is shown in Fig. 4. The dotted line marks the actual tested area. The force required to clamp the specimen between the two halfs of the test-frame is applied by 100 screws. Small cutouts within the corners of the plate (outside the testing area) are necessary there to minimize disturbances of the boundary conditions. The L-direction of the pretreated plate is indicated by arrows.

All panels have been loaded incrementally and monotonicly to different maximum loads. Subsequently different loading paths have been used to get some clues on the behaviour of cyclically loaded shear panels. The maximum loadlevel of all experiments has been low enough to ensure that only small strains could occur.

With regard to the available space, only some crucial points of elasto-plastic, cyclic shear-buckling can be shown. For sake of clearness it seems to be suitable to subdivide the loading history into four parts, the range of

- the first monotonic loading
- load reversal, especially the part near total unloading
- the loading history of further cycles in an undamaged state
- low-cycle-fatigue.

The dimensions of all examined plates were 500 x 500 mm with different thicknesses, varying from 1.0 to 3.0 mm. In the following, the examination is restricted to plates with thickness t = 1.4/1.6 mm. In some cases informations on other tests will be discussed for completion. In Fig. 5 the simplest finite element idealisation is shown. Refined meshes have been used for the examination of higher load levels. All boundaries are clamped. The definition of the angle of shear $\bar{\gamma}$ is given in Fig. 5. The shear-load was applied through inhomogeneous boundary conditions. All computations were performed on an Amdahl 470 V/7, resp. an IBM 3090-600J computer at the Technical University of Braunschweig.

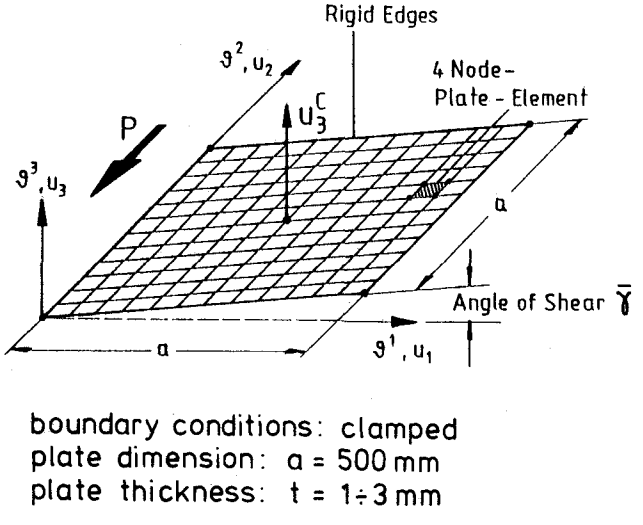

FIG. 5: The idealisation of the problem of a clamped shear-loaded square-plate

3.2 Imperfection sensitivity, buckling behaviour and plastic regions

An undamaged, perfect square-plate will buckle at a certain critical load

$$\tau_{cr.} = k \frac{\pi^2 E^{(el)}}{12(1-\nu^2)} \left(\frac{t}{a}\right)^2 . \qquad (8)$$

k depends on the specific boundary conditions. In case of the clamped square-plate, a neat finite element analysis gives $k = 14.35$. Eqn. (8) may be rearranged to find the critical angle of shear $\gamma_{cr.}$. By using the parameters given in part 3.1, $\gamma_{cr.}$ only depends on the plate thickness t, with

$$\gamma_{cr.} = 0.0078\, t^2$$

and $\gamma_{cr.}$ in [°] and t in [mm]. The undamaged plate will always buckle with the first symmetrical buckling-mode. This buckling-mode corresponds to the lowest eigenvalue.

In case of a real plate initial geometric imperfections will affect the buckling load and the buckling behaviour. For this reason the imperfection sensitivity of the buckling behaviour must be investigated, since it may affect the elasto-plastic deformations. It can be shown by the following figures that in case of a plate with a high aspect-ratio, this is not of interest. Fig. 6 shows some theoretical and experimental results concerning this question. In fig. 6a the influence of the maximum imperfection-amplitude on the buckling behaviour of a plate (thickness $t = 1.4\,mm$) is investigated theoretically, using two different imperfection-modes. One corresponds to the first symmetrical shape-mode, the other one to the second antimetrical shape-mode. In both cases, even if starting with larger imperfections, the influence of them vanishes not later than $\bar{\gamma}/\gamma_{cr.} = 10$. This statement is supported by experimental results, shown in fig. 6b, where the $\bar{\gamma} - u_3^\zeta$-curves for five different test-specimen ($t = 1.4\,mm$) are given. In these cases no pure imperfection-mode (like an shape-mode) is at hand. Two points are relevant in this context: first, as predicted by the theoretical investigation, the infiuence of the imperfection vanishes very soon; second, there is a large amount of different buckling-loads, depending on more or less symmetrical and antimetrical imperfections.

In the case of test PP28, the central deflection u_3^ζ firstly has negative values, before it buckles into the positive direction. This case is related to a very special type of imperfection. The imperfection has a shape, which is similar to a shape-mode of a buckled plate with a shear load in the opposite direction of the actual shear-load. This kind of imperfection results in a short antimetrical, intermediate state (with a high load-level) before it joins the normal symmetrical buckling-mode.

Since the first plastic deformation occurs at about $\bar{\gamma} = 0.2°$ for thin plates of the type mentioned in 3.1, it is unlikely that geometric imperfections will affect the beginning of the plastic onset. Other types of imperfections, e.g. non-homogenious clamping, certainly influence the behaviour of the plates, but they hardly can be examined. Existing small orthotropic, elastic effects may also be neglected, as they do not change the buckling behaviour.

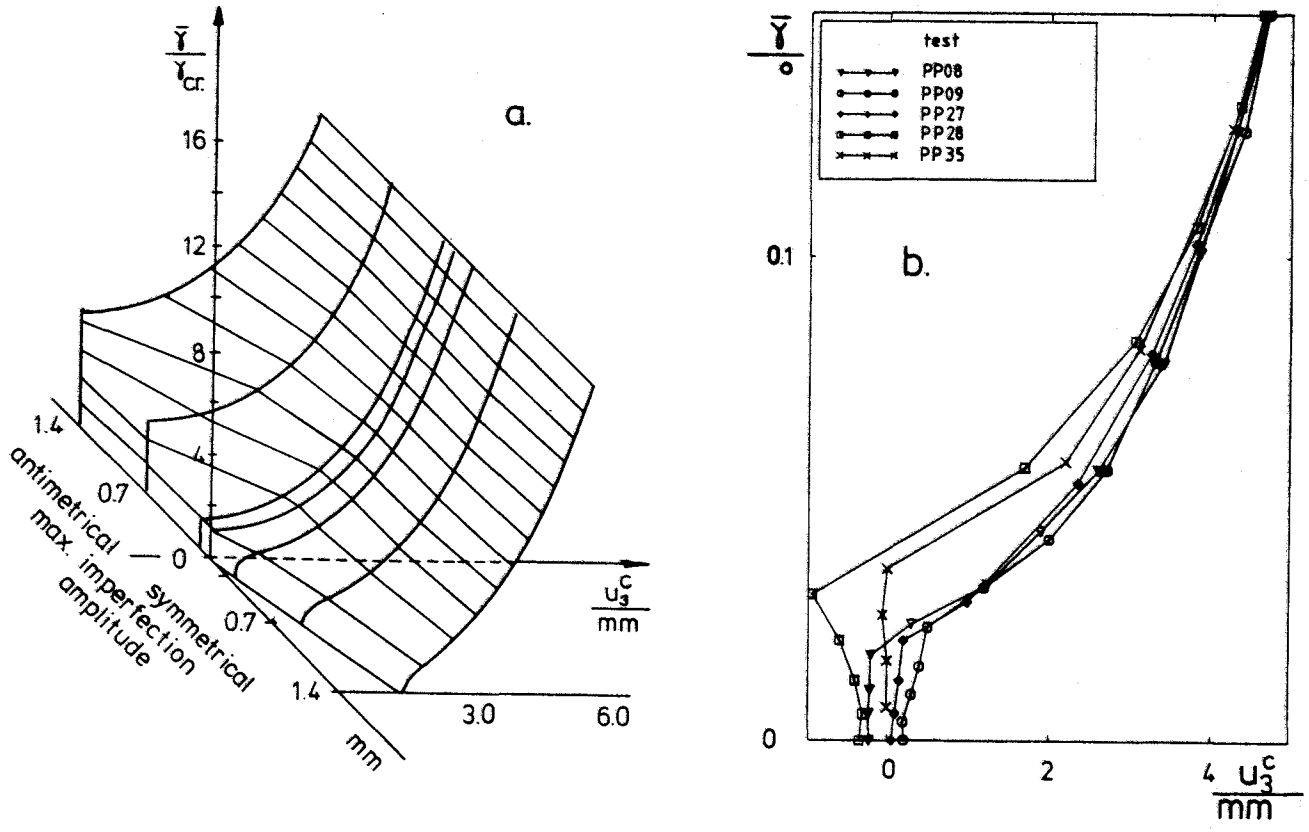

FIG. 6: The imperfection sensitivity :
a. theoretical analysis
b. experimental tests

Fig. 7, in which the angle of shear $\bar{\gamma}$ is plotted versus the central deflection u_3^c, allows a closer look at the buckling-behaviour during the first monotonic loading, of plates of a thickness $t = 1.4\,mm$. Three points shall be discussed in this context. First, filled dots indicate the arithmetic mean of 15 experimental tests and an accompanying horizontal bar indicates the sample variance of each measuring point. It is obvious by the preceding explanations that the large variance in the vicinity of the buckling-load is due to geometric imperfections. On the other hand, the small variance within the higher postbuckling region clearly shows that the influence of these imperfections vanishes with increasing load. A sample variance of $\pm 0.1\,mm$ in the higher postbuckling range may be regarded as very low in case of a buckling problem; as a matter of fact, this value is very near to the estimated tolerance of the measuring-equipment.

Second, the results of two finite element analysises are shown. In the first case a (12 x 12)-element-mesh has been used, in the second case a refined (16 x 16)-mesh. Obviously the results of the (12 x 12)-mesh did not quite converge, but the error is not essential. As the computational effort is about three times higher for the refined mesh, this has been used only in case of very high maximum loads, since a (12 x 12)-mesh would not approximate the buckling-mode in a fair way. The agreement of experimental and theoretical results is very well.

Third, the buckling-pattern is shown in fig. 7 at three selected load-levels. At lower levels, the buckling mode is very much like the corresponding shape-mode of the linear

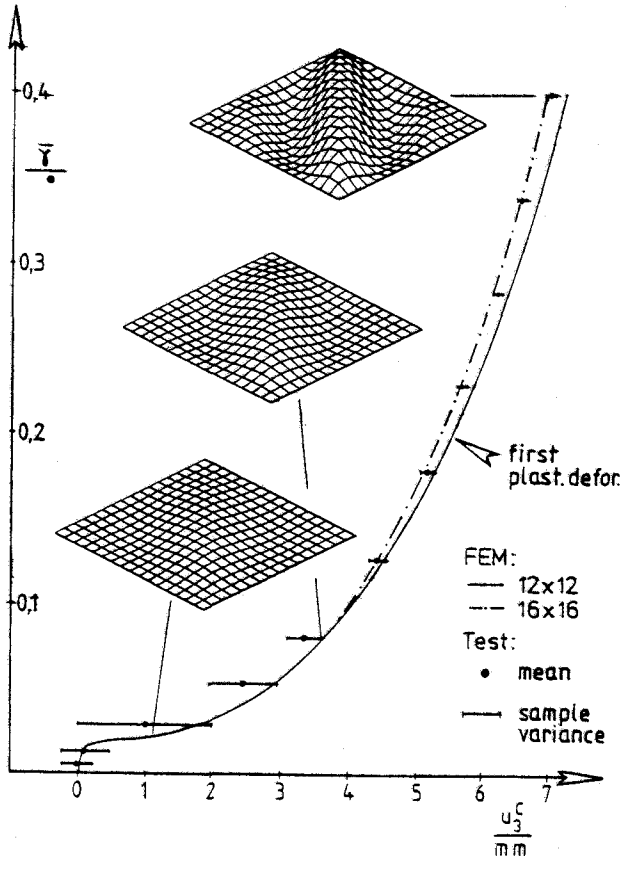

FIG. 7: Buckling-behaviour at first loading ($t = 1.4\,mm$)

stability analysis. Within the higher postbuckling range, additional small buckles appear at the corners of the plates diagonal of compression. This is the reason why a coarse mesh will produce bad results at higher load-levels.

As already mentioned in fig. 7 the first plastic deformations occur at about $\bar{\gamma} = 0.2°$ (this value depends slightly on the used material law). At higher load-levels, the distribution of plasticly deformed knots is exemplarily shown in fig. 8. Each plate has been subdivided into ten layers. Layer 1 corresponds to the lower side of the plate ($\vartheta^3 = -\frac{t}{2}$) and layer 10 to the upper ($\vartheta^3 = \frac{t}{2}$). For comparison the appropriate buckling-mode is shown in a small picture on the upper left side of the figure. The first plastic deformation takes place at a point exactly in front of both corners in the diagonal of tension. This spot is located at layer 1, which is opposite to the ϑ^3-direction of the main buckle. At layer 10 plastic deformations occur just at the edge in the vicinity of the first point.

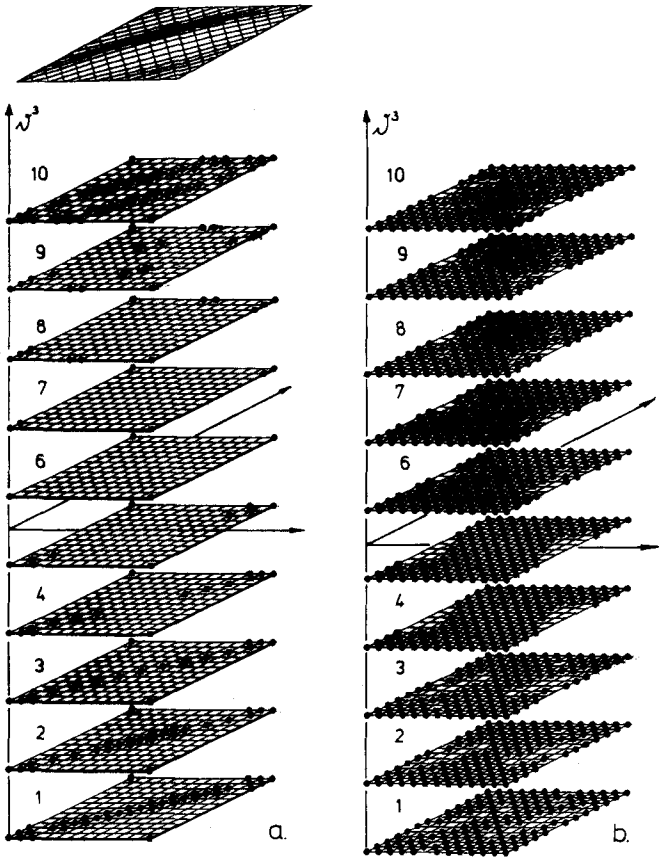

FIG. 8: Distribution of plastic deformations:
a. $\bar{\gamma} = 0.28°$
b. $\bar{\gamma} = 0.39°$

Fig. 8a shows the distribution of plasticly deformed knots at an angle of shear $\bar{\gamma} = 0.28°$. Obviously both points mentioned before as loci of the first plastic deformation are growing up to plastic zones. The starting point expanded just along the diagonal of tension at layer 1. This phenomenon may be striking at first glance since this area is situated "inside" the buckle, but it can be easily explained. Along the diagonal of tension a high negative bending moment m^{12} and a positive shear stress resultant n^{12} act together, due to buckling and shear-load. This results in a high shear stress σ^{12}. At the edges plastic zones grow along the edge and join the plastic zones of the two "side-buckles" (fig. 7). Plastic deformations at the edges are mainly caused by the disturbance of the buckle in this region. In fig. 8a the nonsymmetrical distribution of plastic zones is not strongly developed.

By increasing the angle of shear to $\bar{\gamma} = 0.39°$ (fig. 8b) the plastic zones expand, but this only means that the effects of both mechanisms mentioned above increase. There are three possibilities of expansion: the through-thickness-direction, the plane of the layer and third, the area of new buckles. At this higher load-level, a distinct nonsymmetrical distribution of plasticly deformed knots is obvious; this phenomenon is due to the orthotropic plastic properties of the plate-material. From fig. 8b it becomes also evident that the plate is nearly completely in a plastic state, while $\bar{\gamma} = 0.39°$ is a not so high load-level (this will follow from part 3.3).

3.3 The change of the load-direction

Shear-loaded plates exhibit an unpleasant behaviour during the change of the loading-direction in the vicinity of total unloading. The development of buckles in the opposite loading direction is disturbed, since the developing new buckles are located perpendicular to the buckling-direction of the first monotonic loading. These plastically induced buckles act like geometrical imperfections. But this is not the only disturbance which is valid. At a low load-level, disturbances from other origines (e.g. the clamping) are also very active. Just as in case of geometrical imperfections the influence of these disturbances vanishes after a certain load-level. The vanishing influence of special boundary-conditions can also be proved by theoretical analysis. Because of the already mentioned reasons, the buckling behaviour within the range of load-reversal is affected by the maximum load of the preceding step and the disturbances from other origines. As the magnitude of the second kind of disturbance usually is unknown, it is impossible to predict one certain loading-path in this range.

The sensitivity of this process is also reflected in the $\bar{\gamma} - u_3^c$-curves in fig. 9. The maximum load level at first loading is the only difference between Fig. 9a, b, c and d while all other parameters are the same. All eight panels had a thickness of $t = 1.4mm$. Within each figure the results of two different tests and theoretical analysises are shown. There are always two different loading paths, one with a change of the sign of the central deflection and one without. Since all parameters of all four pairs of tests in fig. 9 have been the same, it is clear that it is necessary to be aware of the fact that there are always two possible pathes at a point of reversal of the load-direction.

In case of small or moderate plastic deformations (due to only moderate maximum loads), a distinct equilibrum-path is given. If either the maximum load is high or large nonsymmetrical disturbances exist, it is very much likely that the plate will get into a special state. This state is outlined in fig. 10 by $\bar{\gamma} - u_3^c$-curves. After a large first

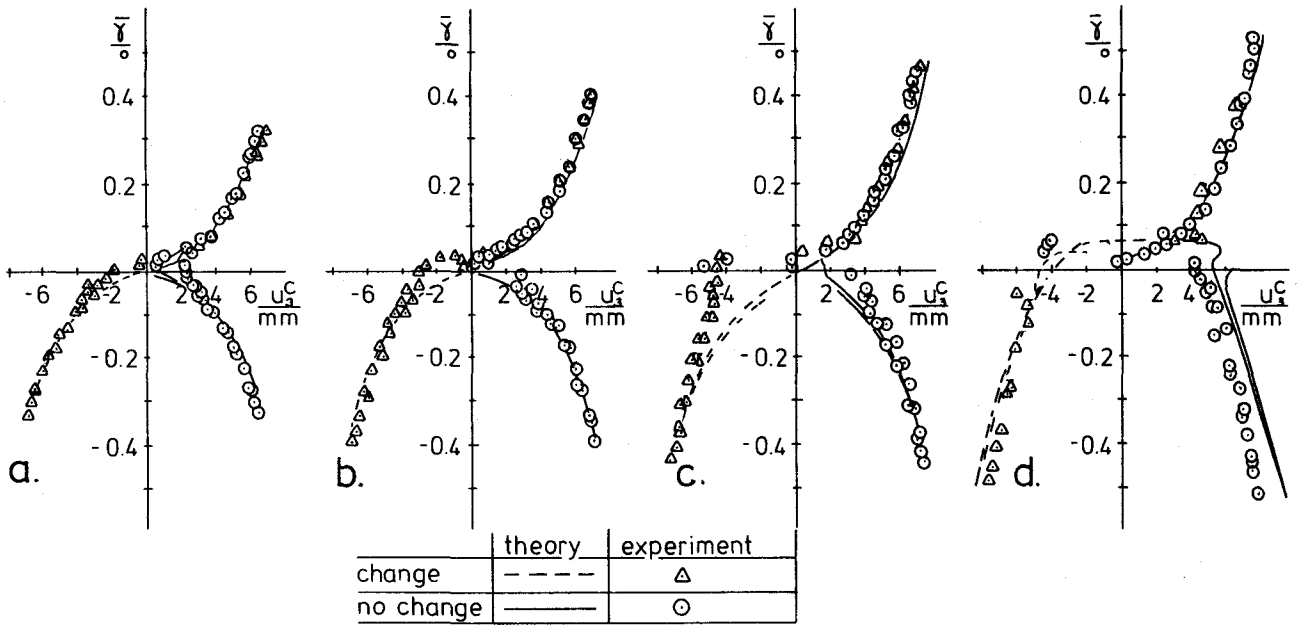

FIG. 9: Buckling behaviour during the first cycle with different first maximum load and different load pathes after total unloading

maximum load, total unloading will occur at a positive angle of shear $\bar{\gamma}$. This point is reached in a predominantly symmetrical buckling-mode. Due to the antimetrical distribution of plastic deformations, the buckling-mode of the following load-path is mainly antimetrical, until a point A is reached. At this point the plate is not able to get into an appropriate buckling-mode without means of a snap-through. This statement is not only valid for experimental studies, it also occurs in theoretical computations, where the analysis detects a limit point and tries to change the direction of loading.

For theoretical computations a change of the loading path has been obtained by using (near the bifurcation point) the corresponding shape-mode as a small geometrical imperfection i.e. disturbance. The agreement of theoretical and experimental results indicates that the used model well describes the real behaviour of the plate and is not influenced by the fact that snap-through is a very fast process, which contradicts the basic requirements of time-independence of the model.

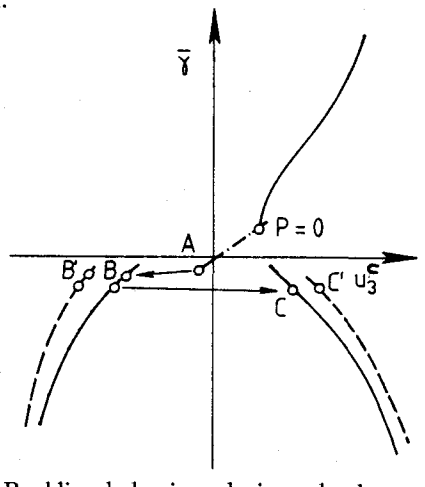

FIG. 10: Buckling-behaviour during a load-reversal after a high maximum load (exemplarily)

As indicated in fig. 10, the snap-through may happen to both, the positive or negative u_3^c-side. Oddly enough, a loading-path with a positive u_3^c-value has nearly always been reached by a *double-snap-through*, if the first maximum load has been high enough. In this case only a short interim-state at the negative side is reached, before the second snap-through gets the buckle back to the preceding position. One more fact is shown in fig. 10: if higher load-levels have been reached during the first monotonic loading, the strength of the snap-through increases (from point B to B' and C to C'). This statement is supported by fig 9 (c and d).

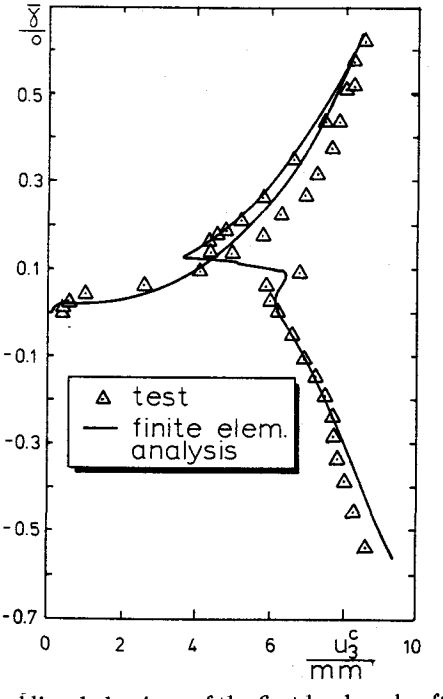

FIG. 11: Buckling-behaviour of the first load-cycle after a high maximum load ($t = 1.6\,mm$), comparison of test- and analytical results

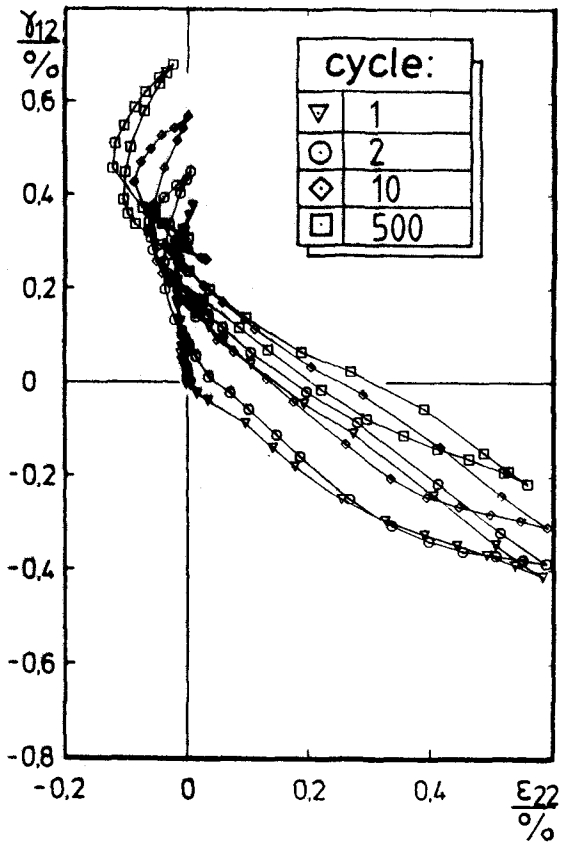

FIG. 12: Strain-path at rosette No. 5 (see figure 4), $\bar{\gamma}_{max} = 0.47^o$, $t = 1.4mm$

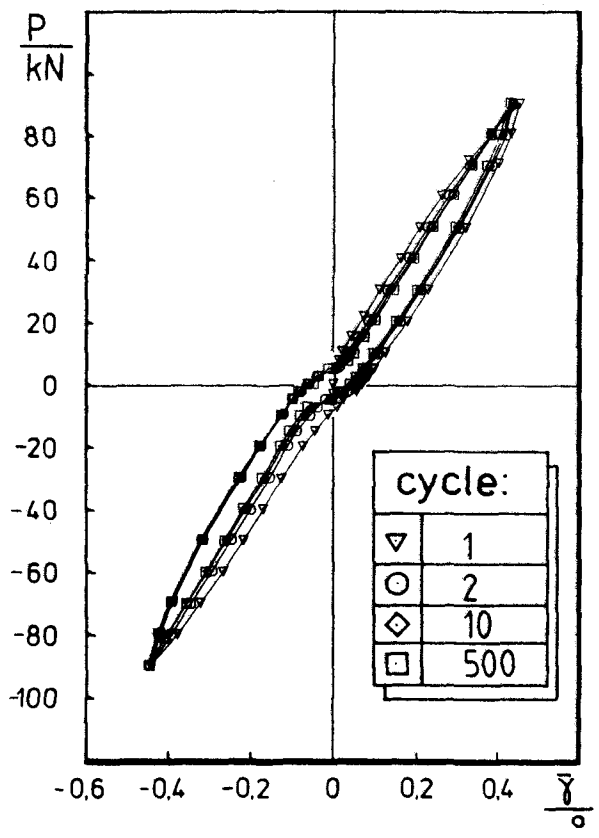

FIG. 13: Load-angle-of-shear-diagramm, $\bar{\gamma}_{max} = 0.47^o$, $t = 1.4mm$

To show the very good performance of this special material model, fig. 11 gives one more example, where a plate ($t = 1.6mm$) has been stressed up to a very high level. To gain a proper approximation at such high loads, it was necessary to use a (16 x 16)-mesh. Two points show how good the theoretical model works. First, the theoretically and experimentally gained value $\bar{\gamma} = 0.13^o$, corresponding to $P = 0\,kN$ agrees very well. Second, the real plate exhibits some kind of a short *blow up* of the buckle, right after the snap-through occured. This is also given by the theoretical model. The blow-up is due to the fact that the *old* buckle lays perpendicular to the *new* diagonal of tension. So it is compressed by a relativly small force, which gets the buckle to swell a bit, before the new buckle has developed. Since this test has been done at an extraordinary high load-level, the results must be judged as a very good agreement of theory and experiment.

3.4 Further Cycles

3.4.1 The uncracked state. As mentioned in the preceding part, the used theoretical model simulates the buckling behaviour very well. Now, two questions appear: first, what are the special requirements set on the elasto-plastic material model to gain such a good approximation and second, what will happen during the next loading-cycles? Both questions are related to each other and may be solved together.

It is substantial for a good performance of a material model, how sensitive it reacts on certain stress;strain-paths. In case of a cyclically shear-buckled plate a great variety of qualitativ different pathes occurs within the whole continuum. Since the attitude of the material model is only discussed in an *integral* way, as the behaviour of the entire plate is investigated, it is not easy to tell which is the critical loading in the continuum. But there are certain features of different material models which support the suggestion that a very special character of buckled plates is responsible for a good or bad approximation by these material-models [3] . It is essential in this context to remind that plastic deformations do not set on before the buckling limit has been exceeded by a considerable factor. Due to this fact it gets clear that the change of the directions of the principle stresses, as it occurs at the buckling-load, is not responsible for a special feature. On the contrary, this change may be neglected here, so that the stress- and strain-paths may be assumed as mainly radial to the origine of the corresponding coordinate system.

Really important is the fact that for many parts of the plate, in the vicinity of the point of total unloading, a complete change of the stress- and strain-direction takes place. Since kinematic hardening is assumed here, such a path implies a non-proportional loading with respect to the kinematically translated yield-surface. Only for highly stressed parts this phenomenon is valid, since only here the translation of the yield-surface is large enough to produce considerable effects. It seems therefore to be essential for the performance of a material model how it copes with this kind of loading. The Mróz-model is very attractive in this context (see e.g. LAMBA ET AL. [11]).

Fig. 12 illustrates the previous statements on typical strain flows and leads to the question: what will happen during the further loading-cycles? In this figure, the strain γ_{12} is plotted versus ε_{22} for a plate ($t = 1.4\,mm$) that has been loaded to $\bar{\gamma}_{max.} = 0.47^o$. The corresponding ε_{11}-component is very near to zero, since the measuring point is situated at the edge of the plate, about 50 mm far from the corner of the plate (at the side of the plate, opposite to the positive u_3^c-direction). This corner is a part of the diagonal of compression at first loading. Curves of four different cycles are shown. In the region discussed here, the largest damage of the material occurs. Two interesting observations can be made:

- the strain-curves migrate to larger values of γ_{12}
- the "hysteresis-loop" gets smaller with a higher number of loading-cycles.

Both remarks reflect that the material properties of this region are considerably changed during the higher loading cycles. But it can be shown that the parts of the plate, where real changes occur, are very small. They are distributed at the edges near the corners of the plate, where the center-buckle of one or the other loading direction interacts with the clamped edges. Obviously these parts are unique in the plate's stress-distribution, since they are highly stressed and the resulting stresses include a high hydrostatic part which is the reason for a large rate of damage. The influence of the change of material properties in these small areas seems to be nearly neglectable, concerning the global buckling behaviour.

The other areas of the plate are not as highly stressed and the hydrostatic part of the stress is much lower. Thus the buckling behaviour of the cycles, except the first one - plastic deformations have to be developed - is very similar. To illustrate this statement, fig. 13 shows the global force P plotted versus the angle of shear $\bar{\gamma}$. The thickness of the plate is $t = 1.4\,mm$. The same statement may be found from $\bar{\gamma} - u_3^c$-curves (e.g. [6]).

The thesis that the influence of small highly deformed regions of the plate on the global buckling behaviour is neglectable, is supported by an even stricter fact. As stated in part 3.3, the u_3^c-direction of the center-buckle may change each time the plate reaches a load-reversal, due to the plastic deformation of the plate and other disturbances. This would imply 2^{2*N} different possible $u_3^c - \bar{\gamma}$-curves, if N is the number of cycles. But this does not happen. From nearly 50 tests that have been conducted, it is learned that the buckling behaviour of the second cycle is exactly equal to the next cycles, as long as cracked parts of the plate are sufficiently small. Regarding that the disturbances are constant, this can only be explained by the fact that - during a fatigue test - changes in the field of the plate and the influence of the edge-parts are neglectably small.

This may be used in theoretical studies. The computational effort needed to investigate geometrically and physically nonlinear problems is very high. Therefore it is impossible to compute a high number of loading cycles. By restricting the examinations of the shear-buckling behaviour to moderate maximum angles of shear ($\bar{\gamma} = 0.6^o$) and to single step tests (SST), the necessity to compute higher numbers of cycles vanishes. The number of cases with different changes of sign of u_3^c reduces from 2^{2*N} to 4 simple types. With the sign of u_3^c at positive resp. negative maximum load you get: $++, --, +-$ and $-+$.

3.4.2 Crackinitiation. The question remains, how long a plate may sustain such relatively high numbers of load-cycles. The work on this subject has just begun, so only a temporary state has been reached. It has already been mentioned in part 3.4.1, at which spots the highest rates of damage will occur. Indeed, crack-initiation always takes place within the area of point 5 (see fig. 4), where the main-buckle interacts with the edge.

To illustrate this problem, the number of loading-cycles $N_{ini.}$ (until crack-initiation) is plotted versus the value of the load-amplitude P in fig. 14a. All specimens had a platethickness $t = 1.4\,mm$ and all tests have been conducted with a relation $R = P_{min}/P_{max} = -1$. It follows from part 3.1 that there is an uncertainty about the real force P, that acts upon the plate (due to friction in the test-frame). A damage has been acknowledged as *initiated crack*, if it reached a length of 2% of the plate-dimension a. A microscope has been used in order to detect cracks as early as possible. All cracks developed directly in the vicinity of the edges. A slight σ^{33}-component (approx. 30 Mpa)

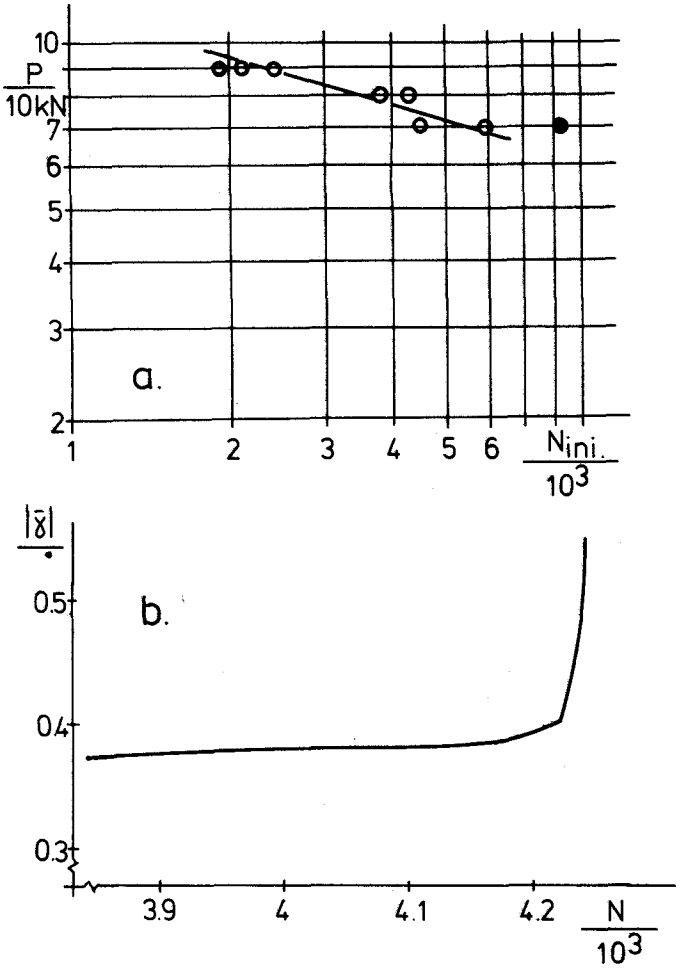

FIG. 14: Durability of shear-loaded plates $t = 1.4\,mm$
a. Crack-initiation
b. Load-capacity after crack-initiation

may influence the durability of the plate, but the interaction of the buckle and the clamped boundary conditions stand out as the main reason of the damage. All tests exhibited a buckling-behaviour with no change of the u_3^c-direction, exept one test, indicated by a filled dot.

From fig. 14a it can be learned that

- also at higher load-levels (plastic deformations set on at about 40 kN) plates exhibit a considerable durability
- although only few tests are available, it seems to be possible that the $P - N_{ini.}$-curve builds nearly a strait line on a logarithmic scale. This has also been found by SINGER ET AL. [1,2] in the case of tests at considerably lower load-levels.

Two more aspects of this problem shall be discussed by using fig. 14b. Fig. 14b shows the curve of the resulting amplitude of the angle of shear $|\bar{\gamma}|$ plotted against the number of loading cycles N. The diagram starts at the moment of crack-initiation and it ends at the fatal point of the complete brake-down of the loading-capacity of the plate. It should be noticed that the amplitude $|\bar{\gamma}|$ at the crack-initiation is just the same as at $N = 2$, so the loading-capacity of the plate for the present remains nearly unchanged by the damage of the areas discribed in 3.4.1. After only a few hundred more cycles there is a total loss of the loading-capacity.

4. Summary

The buckling and postbuckling behaviour of thin-walled aluminium plates has been examined under cyclic shear-load. Experiments have been conducted on a special test set-up for shear-buckling tests. For theoretical investigations a mixed finite element code has been used.

A multi-surface model - based on the one proposed by Mróz - has been applied in order to approximate not only the cyclic behaviour of the material, but also orthotropic, elasto-plastic effects due to the pretreatment of the sheet-metal. The classical rate-independent plasticity theory has been adopted.

Characteristic phenomena of cyclic shear-buckling have been pointed out, as there are: the development of plastic zones, the imperfection sensitivity and the behaviour during load-reversal and at higher numbers of cycles. Crucial points of the theoretical description of the cyclic shear-buckling problem are the existence of bifurcations within the loading path and the appearance of nonproportional stress- and strain-flows.

The comparison of experimental and theoretical results indicated a broad agreement.

ACKNOWLEDGEMENT

The authors gratefully acknowledge the financial support of parts of their investigations by the Deutsche Forschungsgemeinschaft (Sonderforschungsbereich 319) and the Ministerium für Wissenschaft und Kunst des Landes Niedersachsen (durability tests).

References

1. LIBAI, A.; WELLER, T.; KOLLET, M. AND SINGER, J., "Stiffened shear panels subjected to repeated bucklings-durability studies", *TAE-Report* **545**, Haifa, 1984
2. WELLER, T., KOLLET, M., LIBAI, A. AND SINGER, J., "Durability under repeated buckling of stiffend shear panels", *J.Aircraft* **24** (1986) 6-8
3. HORST, P., " Zum Beulverhalten dünner bis in den plastischen Bereich zyklisch durch Schub belasteter Aluminiumplatten", *PhD-Thesis*, Institut für Flugzeugbau und Leichtbau, TU Braunschweig (to appear)
4. TUNKER, H., "Comparison of measured and computed load-deflection behaviour of shear-loaded fiber reinforced plates in the postbuckling range", *Proc. of ICAS 1984*, Paper 84-3.4.3 Toulouse 1984
5. WOLF, K., KOSSIRA, H., "The buckling and postbuckling behaviour of curved laminated shear panels", *Proc. of the* 16^{th} *ICAS-Congress*, Jerusalem 1988
6. HORST, P., KOSSIRA, H., "Theoretical and experimental inverstigation of thin-walled aluminiumpanels under cyclic shearload", in: Proc. International Conferenece:'Spacecraft Structures and Mechanical Testing', Noordwijk, The Netherlands, 19-21 October 1988, *ESA SP* **289** Noordwijk, 1989
7. DAFALIAS, Y., POPOV, I., "Plastic internal variables formalism of cyclic plasticity", *J.Appl.Mech.* **43** (1976) 645-651
8. MRÓZ, Z., "On the description of anisotropic workhardening", *J.Mech.Phys.Solids* **15** (1967) 163-175
9. WOLF, K., "FiPPS ein Programm zur numerischen Analyse des linearen und nichtlinearen Tragverhaltens von Leichtbaustrukturen", in:*ZLR-Bericht* **89-01**, Zentrum für Luft- und Raumfahrt, ed. H.Kossira, TU Braunschweig 1989
10. FROST, R.J.; BENHAM, P.P. "Static and cyclic stress distributions in a buckling shear panel", *J.Strain Anal.* **4** (1969)
11. LAMBA, H.S., SIDEBOTTOM, O.M., "Cyclic plasticity for nonproportional paths: Part 2 - Comparison with predictions of three incremental plasticity models", *J.Engg.Mat.Tech.* **100** (1978) 104-111